Acta Crystallographica Section A
Foundations of Crystallography
ISSN 0108-7673

Received 1 July 2003
Accepted 3 November 2003

Ab initio crystal structure determination using X-ray fluorescence holography for different noise levels: numerical simulation and analysis

F. N. Chukhovskii[a]* and A. M. Poliakov[b]

[a]Institute of Crystallography, Russian Academy of Sciences, 117333 Moscow, Leninsky Prospect 59, Russia, and [b]Department of Materials Science, Moscow Institute of Steel and Alloys, 117279 Moscow, Leninsky Prospect 4, Russia. Correspondence e-mail: fchukhov@hotmail.com

X-ray fluorescence holography (XFH) two-dimensional angular scans with the fluorescing Cu atom of a Cu_3Au single crystal for different noise levels have been calculated and the structure factors have been numerically restored, supporting the *ab initio* structure determination method first discussed by Chukhovskii & Poliakov [*Acta Cryst.* (2003), A**59**, 109–116]. In the case of resultant XFH scans where noise levels are up to the regular signal values at each angular scan point, the elaborated method is found to work well. With the use of the linear regression algorithm code [Chukhovskii & Poliakov *Acta Cryst.* (2003), A**59**, 109–116], the restored structure factors show clearly not just good accuracy of the restoration code procedure but also the efficiency of the structure-determination method that can utilize the XFH data even for high noise levels.

1. Introduction

A classical problem in modern X-ray and electron diffraction techniques is to determine the atomic crystal structure. In the most general case, obtaining a full solution for crystal structures relies on complete faith in theoretical scattering models, which provide insight into the fundamental physics. Among them, the most fruitful model for structure determination purposes is the kinematical theory of the short-wavelength radiation elastic scattering. The latter is utilized in a number of conventional direct methods that decode data from X-ray and/or electron diffraction information, respectively (see *e.g.* Giacovazzo, 1998, for details). For electron diffraction, there are no cases with real samples where the kinematical approximation is rigorously valid and a correct model requires the inclusion of dynamical effects (*e.g.* Marks & Landree, 1998; Hu *et al.*, 2000; Chukhovskii *et al.*, 2001; Chukhovskii & Poliakov, 2003*a*). For instance, Chukhovskii & Poliakov (2003*a*) have developed the 'dynamical' concept of direct methods, combining dynamical electron diffraction and high-resolution transmission-electron-microscopy data, and also the domino type of phase-retrieval algorithm has been proposed, which is capable of yielding a unique phase restoration.

Over the last 15 years, there has been substantial success with the short-wavelength (*e.g.* photoelectrons, fluorescent X-ray quanta) interference technique coupled appropriately with its analysis in terms of Gabor's holography scheme (see Gabor, 1948) and image restoration simulations (see *e.g.* Barton, 1988; Gog *et al.*, 1996; Adams *et al.*, 1998, for references of interest). Just as for photoelectrons, the X-ray fluorescence holography (XFH) data taken over some spherical surface in the reciprocal $\{\mathbf{k}\}$-space can be described as the hologram function $\chi(\mathbf{k}) = [I(\mathbf{k}) - I_0(\mathbf{k})]/I_0(\mathbf{k})$, where $I(\mathbf{k})$ is the X-ray intensity detected for the given wavevector $\mathbf{k}$ and $I_0(\mathbf{k})$ is the corresponding intensity emerging from the fluorescing atom in the absence of an object. Modern XFH schemes utilize incident plane-wave radiation, while fluorescing atoms detect an interference signal. For this, a fluorescence yield depends on both the incident X-radiation direction and its energy, which allows better counting statistics to be obtained (Gog *et al.*, 1995; Novikov *et al.*, 1998; Adams *et al.*, 2000; Chukhovskii *et al.*, 2002).

Noteworthy is the fact that, despite the large number of attempts to utilize the experimental XFH data, very few crystal structures have produced a good image restoration. That is why in many cases of XFH data Barton's multiple energy transform (see *e.g.* Adams *et al.*, 1998; Chukhovskii *et al.*, 2002) has often been 'trial and error'. As is known, the basic Barton transform (Barton, 1988, 1991) was first elaborated to exploit photoelectron holography data. Both the basic and multiple-energy Barton transforms are based on the Helmholtz–Kirchoff integral theorem and suggest that the maxima of the wavefield amplitude distribution match the scattering-atom positions. As far as we know, the Barton transform does nothing for the long-range aims of structure determination but confines itself to the atomic scale imaging of the crystalline unit cell only. It should be mentioned that XFH substantially differs from photoelectron holography not only in the much higher noise level but also because of the

polarization properties of the X-ray spherical waves generated by scattering atoms, which coherently contribute to the holography signal (the two-dimensional angular XFH scan).

In our previous paper (Chukhovskii & Poliakov, 2003*b*, hereafter CHP), we showed how the *ab initio* structure determination method could obtain atomic scale structure information using the XFH data without placing any limits on the structure factors under restoration. In contrast, conventional X-ray diffraction techniques operate using the known (experimental) moduli of structure factors and some mathematical models with limits (*e.g.* phase invariants) imposed on the structure-factor phases. At the same time, although the *ab initio* XFH structure-determination method was successfully proved (CHP), some features, particularly the influence of noise that accompanies the 'regular' XFH angular scan, were beyond the scope of consideration. In fact, the resultant XFH angular scan is a linear superposition of the regular angular scan and a noise and, in the XFH case, the latter can become rather high owing to quite low counting statistics. Despite the generic attraction of the XFH method, the cardinal question arises: what noise level can the *ab initio* structure determination method based on noisy XFH signal data withstand? A prerequisite to solving this issue is to apply the appropriate linear regression algorithm code described in CHP to obtain the atomic scale structure information for different noise levels of the XFH data.

In this paper, the numerical simulations are given for the sample of a Cu_3Au single crystal with fluorescing Cu atom at an energy of 10 keV for the unpolarized incident plane-wave X-radiation and different noise levels. The numerical simulation is carried out within the kinematical scattering approach, according to which the incident plane-wave X-radiation undergoes the first-order scattering at atoms adjacent to the fluorescing Cu atom. One step further, the linear regression algorithm code (CHP) applied for the structure-factor restoration makes clear the noise level values up to which, based on the XFH technique, the *ab initio* structure determination method does work. Noteworthy is the fact that such a study can facilitate the execution of the XFH technique in the field of structural crystallography.

2. Analysis

We will briefly repeat the theoretical analysis for the hologram function $\chi(\mathbf{k})$ (derived in more detail in CHP), aiming to introduce the necessary mathematical formalism.

In the case of unpolarized incident plane-wave X-radiation, the hologram function $\chi(\mathbf{k})$ can be written as follows (*cf.* the corresponding expression in CHP):

$$\begin{aligned}\chi(\mathbf{k}) &= \chi_{\rm reg}(\mathbf{k}) + \delta(\mathbf{k}),\\ \chi_{\rm reg}(\mathbf{k}) &= r_e \int {\rm d}^3\mathbf{r}\,[1 + (\mathbf{n}\cdot\boldsymbol{\kappa})^2]\frac{\cos[k(\boldsymbol{\kappa}\cdot\mathbf{r} + r)]}{r}\rho(\mathbf{r}),\end{aligned} \tag{1}$$

where r_e is the classical radius of an electron, $r_e = 2.818 \times 10^{-15}$ m, $\mathbf{k} = k\boldsymbol{\kappa}$ is the wavevector of the incident plane-wave radiation, $|\boldsymbol{\kappa}| = 1$, $\rho(\mathbf{r})$ is the electron-charge-density (ECD) function of the crystalline medium, $\mathbf{r} = r\mathbf{n}$, $|\mathbf{n}| = 1$, $\chi_{\rm reg}(\mathbf{k})$ and $\delta(\mathbf{k})$ are the regular part and the noise part of the XFH data, respectively. Noteworthy is the fact that the above robust equation (1) for the X-ray hologram function does work if one can neglect the double- and multiple-scattering processes (extinction) of the incident plane-wave radiation.

Further, one uses the Fourier representation of the ECD function $\rho(\mathbf{r})$ as the sum of the reciprocal-space $\rho(\mathbf{h})$ harmonics over the reciprocal diffraction vectors $\mathbf{h}$ as:

$$\rho(\mathbf{r}) = \sum_{\mathbf{h}} \rho(\mathbf{h}) \exp(i\mathbf{h}\cdot\mathbf{r}) \tag{2}$$

and in many cases, for which the kinematical scattering approach will be rather accurate, the ECD $\rho(\mathbf{h})$ harmonics may be replaced by the corresponding structure factor $F(\mathbf{h})$ using the well known relationship (V is a crystal unit-cell volume)

$$\rho(\mathbf{h}) = F(\mathbf{h})/V.$$

By inserting (2) into (1), straightforward evaluations yield the following expression for the regular part of a hologram function (CHP)

$$\begin{aligned}\chi_{\rm reg}(\mathbf{k}) &= \frac{2\pi r_e}{k^2}\sum_{\mathbf{h}} \rho(\mathbf{h}) f(\mathbf{k},\mathbf{h}),\\ f(\mathbf{k},\mathbf{h}) &= f_{\rm spher}(\mathbf{k},\mathbf{h}) + f_{\rm polar}(\mathbf{k},\mathbf{h}),\end{aligned} \tag{3}$$

where each term $\rho(\mathbf{h})f(\mathbf{k},\mathbf{h})$ represents by itself the product of the Fourier ECD $\rho(\mathbf{h})$ harmonics and dimensionless scattering function $f(\mathbf{k},\mathbf{h})$. The latter in turn is the linear superposition of two terms, one of which is polarization independent:

$$f_{\rm spher}(\mathbf{k},\mathbf{h}) = -\frac{k^2}{k^2 - (\mathbf{h}+\mathbf{k})^2} - \frac{k^2}{k^2 - (\mathbf{h}-\mathbf{k})^2} \quad (\mathbf{h} \neq 0); \tag{4}$$

and the other is polarization dependent:

$$\begin{aligned}f_{\rm polar}(\mathbf{k},\mathbf{h}) = {} & \{\ln[-i(k + |\mathbf{h}+\mathbf{k}|)] - \ln[-i(k - |\mathbf{h}+\mathbf{k}|)]\}\\ & \times\left[\frac{3k(k^2 + \mathbf{h}\cdot\mathbf{k})^2}{|\mathbf{h}+\mathbf{k}|^5} - \frac{k^3}{|\mathbf{h}+\mathbf{k}|^3}\right]\\ & - \frac{2k^4(k^2 + \mathbf{h}\cdot\mathbf{k})^2}{|\mathbf{h}+\mathbf{k}|^4(k^2 - |\mathbf{h}+\mathbf{k}|^2)} + \frac{2k^2}{|\mathbf{h}+\mathbf{k}|^2}\\ & - \frac{4(k^2 + \mathbf{h}\cdot\mathbf{k})}{|\mathbf{h}+\mathbf{k}|^4} - \{\ln[i(k - |\mathbf{h}-\mathbf{k}|)]\\ & - \ln[i(k + |\mathbf{h}-\mathbf{k}|)]\}\left[\frac{3k(k^2 - \mathbf{h}\cdot\mathbf{k})^2}{|\mathbf{h}-\mathbf{k}|^5} - \frac{k^3}{|\mathbf{h}-\mathbf{k}|^3}\right]\\ & - \frac{2k^4(k^2 - \mathbf{h}\cdot\mathbf{k})^2}{|\mathbf{h}-\mathbf{k}|^4(k^2 - |\mathbf{h}-\mathbf{k}|^2)} + \frac{2k^2}{|\mathbf{h}-\mathbf{k}|^2}\\ & - \frac{4(k^2 - \mathbf{h}\cdot\mathbf{k})}{|\mathbf{h}-\mathbf{k}|^4}, \quad (\mathbf{h} \neq 0).\end{aligned} \tag{5}$$

Correspondingly, the scattering functions $f_{\rm spher}(\mathbf{k},0)$ and $f_{\rm polar}(\mathbf{k},0)$ are

$$f_{\rm spher}(\mathbf{k},0) = 0.5, \tag{6}$$

$$f_{\rm polar}(\mathbf{k},0) = 2(0.25 - 2 + \mathbf{C} + \ln 2) \cong -0.9593 \tag{7}$$

($\mathbf{C}$ is Euler's constant, $\mathbf{C} \approx 0.5772$).

It should be noted that the dimensionless scattering function $f(\mathbf{k}, \mathbf{h})$ specified by (3)–(5) as a function of wavevector $\mathbf{k}$ contains singularities at the positions of Kossel lines defined by the well known equations $k = |\mathbf{h} \pm \mathbf{k}|$ but not at the 'accidental' points $\mathbf{k} = \pm\mathbf{h}$ by virtue of equations (1) and (2).

For instance, to calculate the correct partial contribution connected with the reciprocal-lattice vector $\pm\mathbf{h}$ to the regular hologram function $\chi_{\rm reg}(\mathbf{k})$, one needs to sum the corresponding terms of $\rho(\mathbf{h})f(\mathbf{k}, \mathbf{h})$ and $\rho(-\mathbf{h})f(\mathbf{k}, -\mathbf{h})$, provided that both the ECD identity of $\rho(\mathbf{h}) = \rho(-\mathbf{h})^*$ and the scattering function identity $f(\mathbf{k}, \mathbf{h}) = f(\mathbf{k}, -\mathbf{h})^*$ hold.

As to the noise of XFH data, the noise is assumed to be accidental for every angular scan point, *i.e.* the noise function contributing to the resultant hologram function [see equation (1)] can be chosen in the form

$$\delta(\mathbf{k}) = \Lambda\,\mathrm{Random}[-1, 1]\chi_{\rm reg}(\mathbf{k}), \qquad (8)$$

where Λ is the noise amplitude (level), the function Random $[-1, 1]$ gives a uniformly distributed pseudorandom real number in the range -1 to 1. With the above noise model, the route-mean-square error $\langle\varepsilon(\mathbf{k})^2\rangle^{1/2}$ of the resultant hologram function $\chi(\mathbf{k})$ at each point $\mathbf{k}$ is equal to $\Lambda|\chi_{\rm reg}(\mathbf{k})|/3$.

As follows from (1), the resultant hologram function $\chi(\mathbf{k})$ is a linear superposition of terms of the type $\rho(\mathbf{h})f(\mathbf{k}, \mathbf{h}) + \rho(\mathbf{h})^* f(\mathbf{k}, \mathbf{h})^*$ and, thus, depends on the moduli and phases of structure-factor amplitudes. It means that the XFH method used to restore the structure factors belongs to the class of *ab initio* structure-determination methods. Recall that in the case of any conventional X-ray diffraction method one deals with the diffraction patterns where only the moduli set, $\{|\rho(\mathbf{h})|\}$, are feasible to measure and for phasing the diffraction pattern one has to use diverse mathematical procedures, each of which in general yields multiple redundant structure solutions.

2.1. Numerical simulation of the noise-contamination-prone XFH angular scans

In practice, the resultant hologram function $\chi(\mathbf{k})$ is obtained in the form of the XFH (θ, φ) scan, where φ is the azimuth angle and θ is the elevation angle of the incident plane-wave radiation [see Fig. 1, recall that $\mathbf{k} \equiv k\boldsymbol{\kappa}(\theta, \varphi)$, where $|\mathbf{k}| = k$ and $|\boldsymbol{\kappa}(\theta, \varphi)| = 1$]. Herein, the numerically simulated XFH (θ, φ) scans with a fluorescing Cu atom of the Cu_3Au structure depending on a different noise level Λ of the noise $\delta(\theta, \varphi)$ scan are put to the test. By virtue of (1)–(8), the XFH (θ, φ) scans are calculated at an energy of 10 keV of the unpolarized

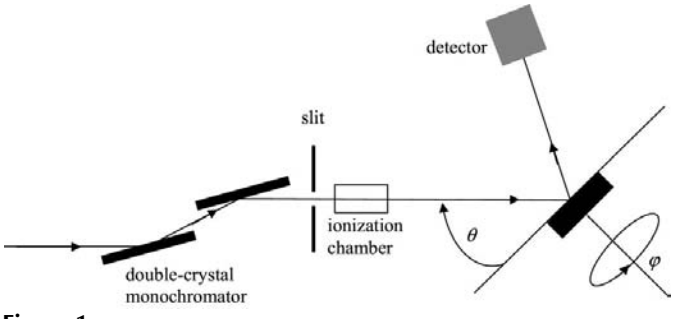

Figure 1
Geometry of obtaining the two-dimensional XFH (θ, φ) scans. The azimuth angle φ and the elevation angle θ are measured with respect to the (001) surface of the Cu_3Au sample.

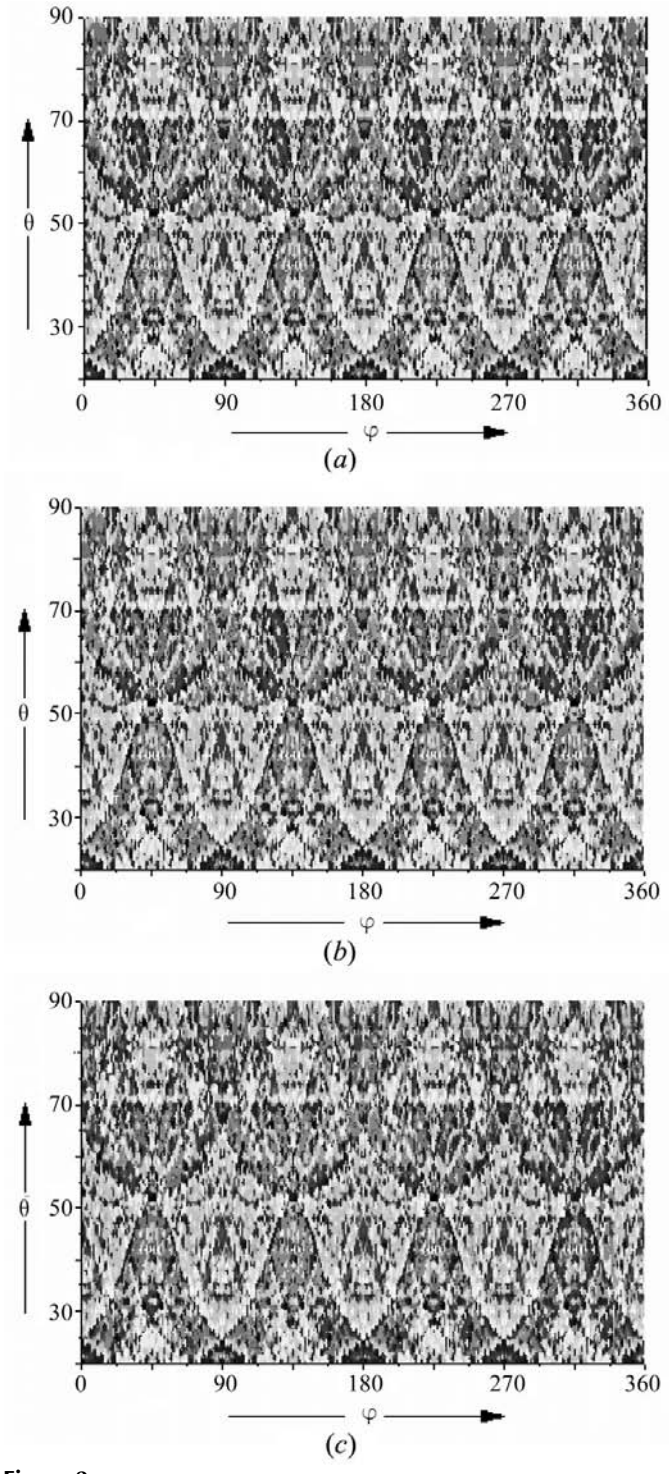

Figure 2
The numerically simulated XFH (θ, φ) scans for 360° azimuth φ, step $\Delta\varphi = 1$, and elevation θ from 20 to 90°, step $\Delta\theta = 1$, at an energy of 10 keV for the incident X-radiation depending on the different noise level Λ equal to: (*a*) 0, (*b*) 0.2, (*c*) 0.6. The total number N of diffraction reflections $(\mathbf{h})$ contributing to the XFH (θ, φ) scans is 243.

incident plane-wave X-radiation for 360° azimuth φ, step $\Delta\varphi$ = 1, and elevation angle θ varies from 20 to 90°, step $\Delta\theta$ = 1. The simulated XFH scan examples are displayed in Fig. 2 for Λ = 0, 0.2, 0.6 and in Fig. 3 for Λ = 1, 2, 6 for the total number N of true structure factors $F_{\rm true}(\mathbf{h})$ equal to 243. Owing to the $m3m$ point symmetry of the Cu_3Au structure, among the total number of 243 structure factors $F_{\rm true}(\mathbf{h})$, only 25 structure factors are crystallographically different, and only 22 of them are different valued because the values of the structure amplitudes for pairs of crystallographic planes of {003} and {212}, {104} and {223}, {303} and {114} types do not differ from each other.

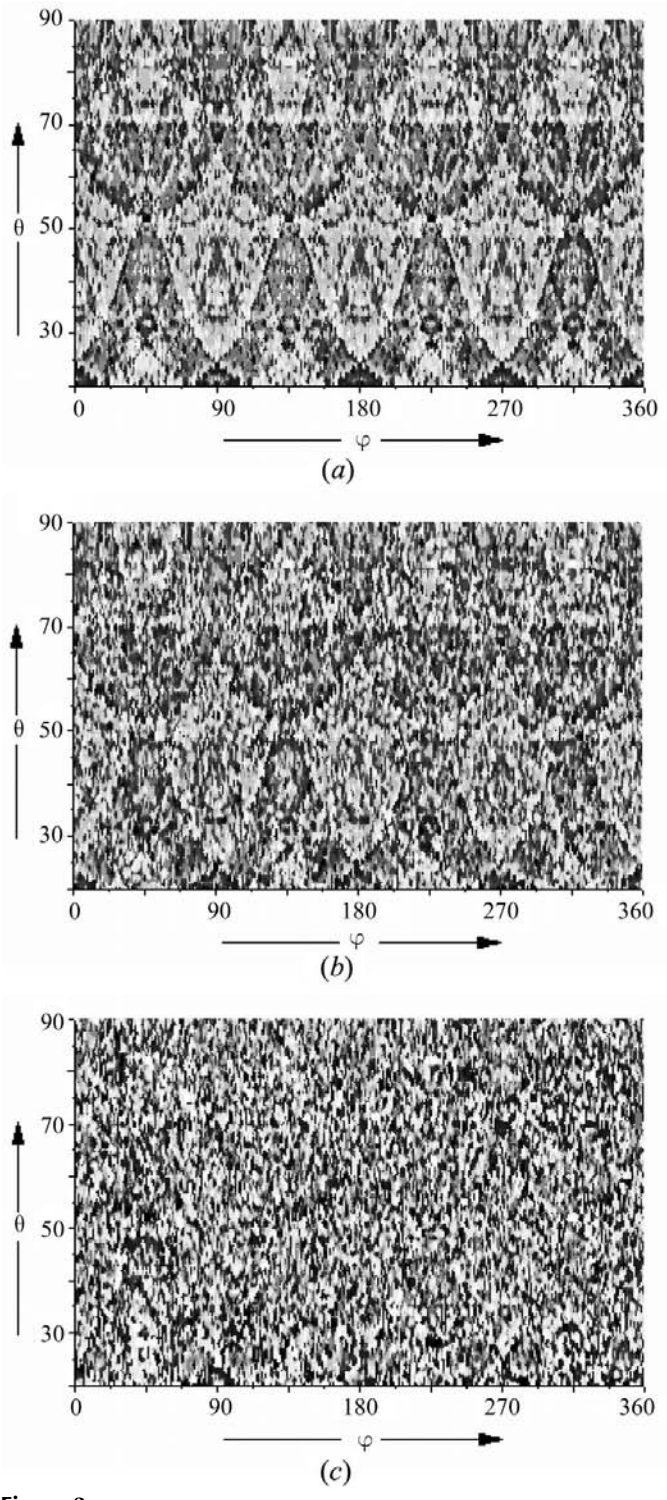

Figure 3
The numerically simulated XFH (θ, φ) scans for 360° azimuth φ, step $\Delta\varphi$ = 1, and elevation θ from 20 to 90°, step $\Delta\theta$ = 1, at an energy of 10 keV of the incident X-radiation depending on the different noise level Λ equal to: (*a*) 1, (*b*) 2, (*c*) 6. The total number N of diffraction reflections (**h**) contributing to the XFH (θ, φ) scans is 243.

The cases (*a*)–(*c*) of Figs. 2 and 3 are related to the numerical values 0, 0.2, 0.6 and 1, 2, 6 of the noise amplitude Λ, respectively. Generally, depending on the noise level Λ, the simulated XFH patterns are the noise-contamination-prone superposition of Kossel's lines $k = |\mathbf{h} \pm \mathbf{k}|$ related to the different reciprocal-lattice vectors **h**, the total number of which is equal to 243 (*cf.* CHP). In the case of Λ = 0, because of the fourfold-axis symmetry around the [001] direction and mirror plane normal to the [110] direction for the Cu_3Au crystal structure, the XFH (θ, φ) scans possess the azimuth '90 degree translation' symmetry, and each fourth part of the XFH (θ, φ) scans has the azimuth '45 degree symmetry' (*cf.* Fig. 2*a* herein, and Fig. 5*c* in CHP). It is clearly seen that up to Λ = 1 the XFH (θ, φ) scans (see Figs. 2*a*–*c*, Fig. 3*a*) keep the general features of the gauge (regular) XFH (θ, φ) scan of Fig. 2(*a*) for Λ = 0. Then, with further increasing Λ they turn into rambling ones far from the gauge scan displayed in Fig. 2(*a*).

2.2. Structure-factor restoring: least-squares method and statistical errors estimation

To examine the XFH structure determination method, one formulates the issue as restoring structure factors $F_{\rm true}(\mathbf{h})$ by the use of the resultant XFH (θ, φ) scans numerically simulated (see Figs. 2 and 3) and treated as the known ones, $\chi_{ij} \equiv \chi(\theta_i, \varphi_j)$ at each two-dimensional point (θ_i, φ_j), which depend on the noise level Λ. Given an estimate for the structure amplitudes generated by a standard least-squares method, consider a χ^2 form under minimization, namely:

$$\chi^2 = \left[\sum_{i,j} (\chi_{ij} - \chi_{{\rm reg},ij})^2 / \langle \varepsilon_{ij}^2 \rangle \right]_{\rm min} \tag{9}$$

and the following notations are introduced:

$$\chi_{{\rm reg},ij} \equiv \chi_{\rm reg}(\theta_i, \varphi_j), \quad \langle \varepsilon_{ij}^2 \rangle \equiv \langle \varepsilon^2(\theta_i, \varphi_j) \rangle.$$

Correspondingly, equation (9) reduces to the matrix equation for the structure factors:

$$\widehat{\mathbf{A}}\mathbf{F} = \mathbf{B}, \tag{10}$$

where the symmetric matrix $\widehat{\mathbf{A}}$ and the column vector **B** are introduced by

$$\begin{aligned} \hat{\mathbf{A}} &= A(\mathbf{h}, \mathbf{g}), \quad & A(\mathbf{h}, \mathbf{g}) &= \sum_{ij} \frac{f_{ij}(\mathbf{h}) f_{ij}(\mathbf{g})}{\langle \varepsilon_{ij}^2 \rangle}, \\ \mathbf{B} &= B(\mathbf{h}), & B(\mathbf{h}) &= \sum_{ij} \frac{\chi_{ij} f_{ij}(\mathbf{h})}{\langle \varepsilon_{ij}^2 \rangle}, \end{aligned} \tag{11}$$

the elements of which are $f_{ij}(\mathbf{h}) \equiv f(\theta_i, \varphi_j; \mathbf{h})$. The column vector $\mathbf{F}$ consists of the restored structure factors $F_{\rm rest}(\mathbf{h})$ for different reciprocal-lattice vectors $\mathbf{h}$.

As follows from (11), each matrix element $A(\mathbf{h}, \mathbf{g})$ is the linear superposition of the bilinear product of the scattering functions, $f_{ij}(\mathbf{h})\, f_{ij}(\mathbf{g})$, divided by the mean square $\langle \varepsilon_{ij}^2 \rangle$ whereas the column element $B(\mathbf{h})$ is the linear superposition of the normalized resultant XFH scan functions $\chi_{ij}/\langle \varepsilon_{ij}^2 \rangle^{1/2}$ weighted with the normalized scattering functions $f_{ij}(\mathbf{h})/\langle \varepsilon_{ij}^2 \rangle^{1/2}$.

By substituting the noise function, $\delta_{ij} \equiv \delta(\theta_i, \varphi_j)$, into the right-hand side of the second equation of (11) and assuming the noise measured is statistically independent for all 'each-to-each' scan points, one easily finds that the discrete correlation function $\langle B(\mathbf{h})B(\mathbf{g}) \rangle$ evaluated for the two reciprocal-lattice vectors $\mathbf{h}$ and $\mathbf{g}$ is equal to

$$\langle B(\mathbf{h})B(\mathbf{g}) \rangle = A(\mathbf{h}, \mathbf{g}), \tag{12}$$

i.e., in other words, the discrete correlation function $\langle B(\mathbf{h})B(\mathbf{g}) \rangle$ is simply equal to the matrix element $A(\mathbf{h}, \mathbf{g})$ of the basic matrix equation (9) for restoring the structure factor by use of the resultant XFH χ_{ij} scan.

Equation (12) instantly allows the discrete covariant matrix of the 'structure-factor errors' to be obtained. Indeed, the discrete covariant matrix $\langle \delta F(\mathbf{h}) \delta F(\mathbf{g}) \rangle$ of 'structure-factor errors' can be written as follows:

$$\langle \delta F(\mathbf{h}) \delta F(\mathbf{g}) \rangle = (\widehat{\mathbf{A}}^{-1})_{\mathbf{hg}}. \tag{13}$$

To be specific, in the frame of our noise model where the XFH noise is statistically independent for all 'each-to-each' scan points measured, the discrete covariant matrix $\langle \delta F(\mathbf{h}) \delta F(\mathbf{g}) \rangle$ of discrete 'structure-factor errors' is determined by the inverse matrix of the basic equation (9). For reference, the given approach to obtain 'structure-factor errors' may be compared with the corresponding one of the 'structure-factor error' equations [see (15)–(18) in CHP], which exploit the χ^2 minimization for the structure-factor errors.

Using this strategy, based on (9), we then determined the structure-factor vector $\mathbf{F}$ by applying the linear regression procedure (CHP) and the discrete covariant matrix $\langle \delta F(\mathbf{h}) \delta F(\mathbf{g}) \rangle$ of 'structure-factor errors' in accordance with (13). This procedure is used for determining all the 243 structure factors that contribute to the numerically simulated resultant XFH $\chi(\theta, \varphi)$ scans under some particular realization of the noise random function (8) with the different noise levels Λ between 0 and 10 (see *e.g.* Figs. 2, 3).

The final results for the relative errors of the restored structure factors, $\gamma(\mathbf{h}) \equiv |\Delta F(\mathbf{h})/F_{\rm true}(\mathbf{h})|$, $\Delta F(\mathbf{h}) = F_{\rm rest}(\mathbf{h}) - F_{\rm true}(\mathbf{h})$ [except $\gamma(\mathbf{h})$ for $\mathbf{h} = 0$] are shown in Fig. 4 as a histogram for the noise level range Λ from 0 to 6. The values of $\overline{\gamma(\mathbf{h})}$ averaged over the crystallographically equivalent reflections of the given Cu_3Au structure are listed in Table 1. The normalized discrete-covariant matrix $\langle \delta F(\mathbf{h}) \delta F(\mathbf{g}) \rangle / [\langle \delta F(\mathbf{h})^2 \rangle^{1/2} \langle \delta F(\mathbf{g})^2 \rangle^{1/2}]$ is built in Fig. 5 as a two-dimensional diagram. Notice that in accordance with the chosen noise model (8) each of the elements of $\langle \delta F(\mathbf{h}) \delta F(\mathbf{g}) \rangle$ is proportional to the noise level squared. All the diagonal elements of $\langle \delta F(\mathbf{h})^2 \rangle$ are dominant, giving an idea of the mean-square errors of the structure factors of restoration. Noteworthy is the fact that equation (13) for estimating $\langle \delta F(\mathbf{h}) \delta F(\mathbf{g}) \rangle$ monitors the progress of restoring the plausible structure factors using the resultant XFH $\chi(\theta, \varphi)$ data.

The calculated data herein clearly reflect all the intrinsic features of the noise model that affects the resultant XFH $\chi(\theta, \varphi)$ scans. Evident are all the main details of the growth of relative errors $\gamma(\mathbf{h})$ with increasing noise level Λ (see Fig. 4). This is even more apparent for the correspondingly averaged errors $\overline{\gamma(\mathbf{h})}$ listed in Table 1. With the XFH method for structure determination inserted into context, the errors

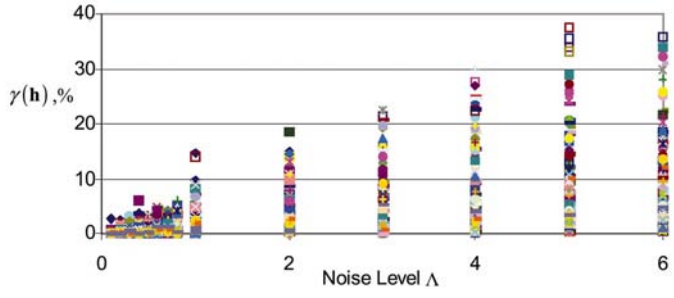

Figure 4
Histogram of the relative errors of the structure factors restored, $\gamma(\mathbf{h}) \equiv |\Delta F(\mathbf{h})/F_{\rm true}(\mathbf{h})|$, $\Delta F(\mathbf{h}) = F_{\rm rest}(\mathbf{h}) - F_{\rm true}(\mathbf{h})$ [except $\gamma(\mathbf{h})$ for $\mathbf{h} = 0$] for the noise level range Λ from 0 to 6.

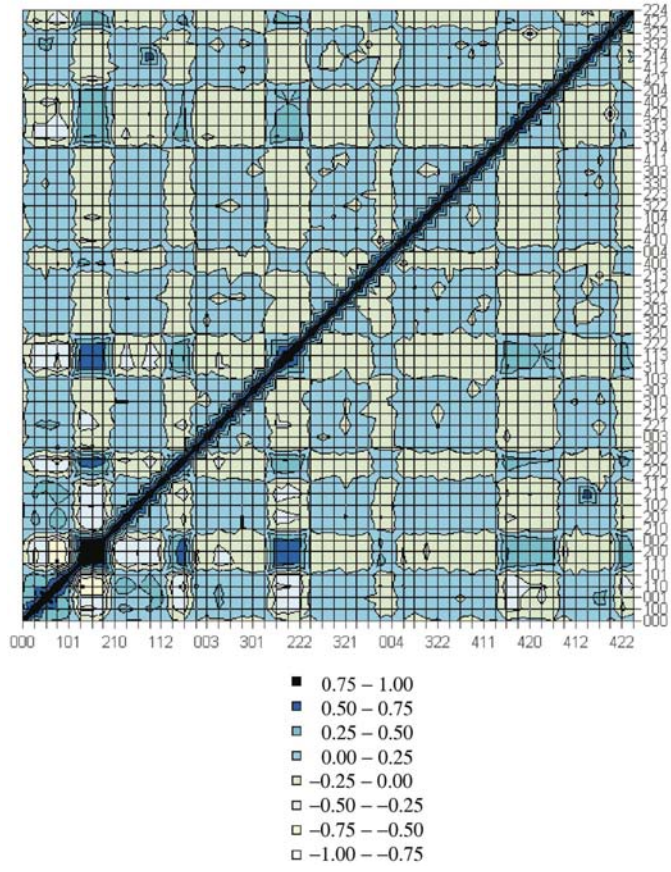

Figure 5
Diagram of the normalized discrete covariant matrix $\langle \delta F(\mathbf{h}) \delta F(\mathbf{g}) \rangle / \langle \delta F(\mathbf{h})^2 \rangle^{1/2} \langle \delta F(\mathbf{g})^2 \rangle^{1/2}$ of the 'structure-factor errors' calculated with equation (13).

Table 1
Averaged relative errors, $\overline{\gamma(\mathbf{h})}$ (%), of the restored structure factors $F_{\rm rest}(\mathbf{h})$ depending on different values of the noise level Λ.

The values $\overline{\gamma(\mathbf{h})}$ are averaged over the crystallographically equivalent reflections of the Cu_3Au structure. The double-valued $\overline{\gamma(\mathbf{h})}$ for the noise level $\Lambda = 1$ are given to illustrate the effect of the two different realizations of the random noise function (8).

	Noise level Λ															
$h = \{HKL\}$	0.1	0.2	0.3	0.4	0.5	0.6	0.7	0.8	1.0	1.0	2.0	3.0	4.0	5.0	6.0	10.0
000	2.65	2.53	2.66	3.71	0.63	1.97	1.59	3.43	9.64	14.69	15.03	0.83	17.19	105.04	110.66	114.55
010	0.02	0.25	0.37	0.09	0.28	0.11	0.05	0.06	0.26	0.47	0.81	0.12	3.24	1.88	1.17	5.78
$\bar{1}10$	0.00	0.21	0.16	0.26	0.28	0.48	0.12	0.08	0.22	0.18	0.02	0.05	0.41	0.48	2.02	5.06
$\bar{1}\bar{1}1$	0.01	0.20	0.23	0.11	0.13	0.32	0.04	0.20	0.10	0.39	0.63	0.52	0.41	0.62	2.89	3.86
020	0.02	0.17	0.17	0.11	0.03	0.38	0.03	0.08	0.17	0.34	0.43	0.57	0.85	0.46	2.66	3.53
$\bar{2}10$	0.00	0.17	0.28	0.26	0.11	0.45	0.03	0.19	0.54	0.36	0.82	0.39	2.12	1.81	2.29	0.10
$\bar{2}\bar{1}1$	0.08	0.21	0.25	0.10	0.01	0.11	0.04	0.18	0.43	0.44	0.75	0.27	0.23	1.08	1.95	0.58
$\bar{2}20$	0.07	0.24	0.02	0.27	0.33	0.22	0.08	0.36	0.24	0.21	0.03	0.20	0.23	0.59	2.27	4.66
030	0.11	0.26	0.64	0.04	0.12	0.69	0.80	0.62	2.11	0.57	0.48	0.29	0.40	1.00	0.82	7.22
$\bar{2}\bar{2}1$	0.03	0.09	0.01	0.22	0.38	0.14	0.47	0.18	0.29	0.13	0.42	1.64	1.69	1.69	2.44	2.83
$\bar{3}10$	0.06	0.35	0.06	0.69	0.33	0.18	0.29	0.58	0.51	0.04	0.41	1.82	2.22	1.70	0.06	5.74
$\bar{3}\bar{1}1$	0.02	0.20	0.10	0.16	0.24	0.26	0.01	0.21	0.18	0.16	0.56	0.27	0.98	1.21	2.49	4.22
$\bar{2}\bar{2}2$	0.03	0.13	0.01	0.19	0.23	0.08	0.03	0.33	0.39	0.17	0.38	0.42	0.72	2.39	0.75	3.94
$\bar{3}20$	0.05	0.35	0.13	0.02	0.31	0.31	0.87	0.00	0.45	1.39	1.84	2.69	3.05	10.54	6.01	6.37
$\bar{3}\bar{2}1$	0.01	0.33	0.00	0.06	0.64	0.07	0.37	0.67	0.30	0.85	1.06	0.88	6.95	0.12	0.71	4.78
040	0.10	0.28	0.23	0.05	0.45	0.51	0.30	0.16	0.23	0.09	0.51	0.83	2.43	3.03	5.12	3.51
$\bar{4}10$	0.06	0.12	0.26	0.14	0.53	0.90	0.30	0.32	0.72	1.28	3.21	0.16	0.63	1.48	1.85	7.04
$\bar{3}\bar{2}2$	0.02	0.05	0.01	0.71	0.25	0.63	0.21	0.29	0.21	0.01	2.07	0.77	0.02	8.79	0.65	5.19
$\bar{3}30$	0.03	0.21	0.13	0.38	0.44	0.34	0.23	0.70	0.48	0.08	0.59	0.09	3.40	3.07	0.19	3.64
$\bar{4}\bar{1}1$	0.11	0.31	0.00	0.33	0.61	0.23	0.15	1.58	0.45	0.91	2.00	3.56	0.48	7.47	2.37	0.94
$\bar{3}\bar{3}1$	0.04	0.23	0.24	0.09	0.08	0.50	0.08	0.11	0.30	0.11	0.10	0.07	0.36	1.02	1.19	3.05
$\bar{4}20$	0.00	0.28	0.02	0.27	0.07	0.57	0.28	0.09	0.47	0.27	0.77	0.11	2.80	2.13	0.25	2.73
$\bar{4}\bar{2}1$	0.11	0.20	0.17	0.91	0.57	0.67	0.11	0.60	2.19	0.09	1.67	0.90	2.44	4.46	6.54	1.67
$\bar{3}\bar{3}2$	0.03	0.20	0.12	0.01	0.09	0.54	0.15	0.52	0.11	0.51	0.14	0.22	4.42	0.83	6.02	2.23
$\bar{4}\bar{2}2$	0.02	0.19	0.24	0.02	0.05	0.40	0.02	0.28	0.07	0.39	0.71	1.55	1.18	0.52	0.69	1.67

Table 2
Summary of results for the r.m.s. structure-factor errors in the case of the crystallographically equivalent reflections of type {100}, {110}, {111} and {002} of the Cu_3Au structure for some realization of the random noise function (8) with the noise level $\Lambda = 1$; $\gamma(\mathbf{h}) \equiv |\Delta F(\mathbf{h})/F_{\rm true}(\mathbf{h})|$, $\Delta F(\mathbf{h}) = F_{\rm rest}(\mathbf{h}) - F_{\rm true}(\mathbf{h})$ is the relative (non-averaged) error of the restored structure factor $F_{\rm rest}(\mathbf{h})$ with noise level $\Lambda = 1$ (*cf.* column 10 of Table 1).

h					
H	K	L	$F_{\rm true}(\mathbf{h})$	$\gamma(\mathbf{h})$ (%)	$\langle\delta F(\mathbf{h})^2\rangle^{1/2}/\lvert F_{\rm true}(\mathbf{h})\rvert$ (%)
0	0	0	165.94	9.64	21.41
0	1	0	−15.58	0.14	1.05
1	0	0		0.33	1.05
0	0	1		0.58	1.26
−1	1	0	−14.75	0.02	0.78
1	1	0		0.11	0.78
−1	0	1		0.22	1.29
0	−1	1		0.29	1.28
0	1	1		0.17	1.28
1	0	1		0.93	1.28
−1	−1	1	131.92	0.05	0.69
−1	1	1		0.03	0.69
1	−1	1		0.16	0.69
1	1	1		0.14	0.69
0	2	0	125.15	0.09	0.70
2	0	0		0.29	0.70
0	0	2		0.12	0.74

directly illustrate that while the noise level Λ is less than and/or around unity, most structure amplitudes are restored with accuracy better than 10% [Table 1, except the value of $F(0)$] and this result may be independent of the noise model used. Our calculations show that although noise makes the resultant XFH $\chi(\theta, \varphi)$ scans rambling, at the same time it does not strongly affect the accuracy of the restored structure factors. Presumably, this result is independent of the noise model since the positions and black–white contrast of Kossel lines, which have a sense, are stable against the noise of the XFH patterns (*cf.* Figs. 2, 3).

3. Discussion and concluding remarks

In this paper, we pursued the purpose of proposing the XFH method as an *ab initio* technique for obtaining atomic scale information even if the noise in the XFH $\chi(\theta, \varphi)$ data was rather high. The examples of the structure-factor determination carried out by use of numerically simulated XFH $\chi(\theta, \varphi)$ data for the fluorescing Cu atom of the Cu_3Au structure and different levels of noise lead to the following solid conclusion. Even if noise composes a significant part of the XFH patterns, for instance due to low counting statistics, the XFH method provides a robust unambiguous procedure for determining plausible structure factors with quite a good accuracy. Besides, it is essential that, as conventional X-ray diffraction techniques use rather complicated and sophisticated mathematical models, the said XFH method uses the linear regression algorithm code (CHP).

Major restrictions on the implementation of the XFH method to X-ray structure determination were analysed in our previous paper (CHP). In particular, the kinematical scat-

tering approach and the corresponding basic scattering functions used in our treatment, polarization and coherence properties of the incident X-radiation, sample sizes and, especially, the so-called 'average' sets of restored structure factors feasible from the XFH data obtained with the fluorescing Cu atom of the Cu_3Au structure were analysed.

In conclusion, herein we draw attention to the peculiar properties of *a priori* estimates of the structure-factor errors based on (13). Apart from the noise level, the discrete covariant matrix $\langle \delta F(\mathbf{h}) \delta F(\mathbf{g}) \rangle$ is determined by a product of the scattering functions $f(\mathbf{k}, \mathbf{h})$ and $f(\mathbf{k}, \mathbf{g})$ only related to the regular XFH data. It does imply that the number of different mean-square errors $\langle \delta F(\mathbf{h})^2 \rangle$ even for crystallographically equivalent reflections is governed by an *ad hoc* symmetry of the complete system consisting of the 'external' XFH set-up (without a sample, see Fig. 1) and the Cu_3Au structure sample (Curie's principle, see *e.g.* Nye, 1957). As an example, we consider such a situation with the structure factors related to the reflections of {100} and {110} types of Cu_3Au structure (Table 2, for the sake of simplicity we put $\Lambda = 1$). As is seen, the r.m.s. structure-factor errors differ for the reflections 001 and 100 and they coincide for the reflections 100 and 010. The reflections of {110} type demonstrate similar behavior. These are a direct consequence of Curie's principle. In fact, by virtue of the accepted XFH $\chi(\theta, \varphi)$ geometry with fixed angular steps along both the azimuth φ and polar θ directions, the 'external' set-up has 360*mm* point symmetry whereas the Cu_3Au structure has *m*3*m* point symmetry. Correspondingly, Curie's principle claims that the complete system of a sample and 'external' set-up has the point symmetry that is the intersection of both the individual point symmetries. In our case, we have 360*mm* and *m*3*m* and their intersection gives the 4*mm* point symmetry since $4mm = 360mm \cap m3m$. As a result, from the physics viewpoint, the reflections 010 and 100 are equivalent, while the reflections 100 and 001 are not and so similarly are the reflections of {110} type and {200} type, whereas all the {111} reflections are equivalent (see Table 2 for details).

In concluding, we would like to claim that the feasibility and capability of the linear regression code, even when there is a rather high noise level, should be a persuasive argument for obtaining atomic scale information on crystalline materials by the *ab initio* XFH technique with quite low counting statistics.

References

Adams, B., Nishino, Y. & Materlik, G. (2000). *J. Synchrotron Rad.* **7**, 274–279.

Adams, B., Novikov, D. V., Hiort, T., Kossel, E. & Materlik, G. (1998). *Phys. Rev. B*, **57**, 7526–7534.

Barton, J. J. (1988). *Phys. Rev. Lett.* **61**, 1356–1359.

Barton, J. J. (1991). *Phys. Rev. Lett.* **67**, 3106–3109.

Chukhovskii, F. N., Hu, J. J. & Marks, L. D. (2001). *Acta Cryst.* A**57**, 231–239.

Chukhovskii, F. N., Novikov, D. V., Hiort, T. & Materlik, G. (2002). *Opt. Commun.* **209**, 273–277.

Chukhovskii, F. N. & Poliakov, A. M. (2003*a*). *Acta Cryst.* A**59**, 48–53.

Chukhovskii, F. N. & Poliakov, A. M. (2003*b*). *Acta Cryst.* A**59**, 109–116.

Gabor, D. (1948). *Nature (London)*, **161**, 777–780.

Giacovazzo, C. (1998). *Direct Phasing in Crystallography. Fundamentals and Applications.* Oxford University Press.

Gog, T., Bahr, D. & Materlik, G. (1995). *Phys. Rev. B*, **51**, 6761–6764.

Gog, T., Menk, R. H., Arfelli, F., Len, P. M., Fadley, C. S. & Materlik, G. (1996). *Synchrotron Rad. News*, **9**, 30–35.

Hu, J. J., Chukhovskii, F. N. & Marks, L. D. (2000). *Acta Cryst.* A**56**, 458–469.

Marks, L. D. & Landree, E. (1998). *Acta Cryst.* A**54**, 296–305.

Novikov, D. V., Adams, B., Hiort, T., Kossel, E., Materlik, G., Menk, R. & Walenta, A. (1998). *J. Synchrotron Rad.* **5**, 315–319.

Nye, J. F. (1957). *Physical Properties of Crystals.* Oxford: Clarendon Press.